Structure and Dynamics of the Membrane-Embedded Domain of LmrA Investigated by Coupling Polarized ATR-FTIR Spectroscopy and $^1H/^2H$ Exchange†

Vinciane Grimard,‡ Catherine Vigano,‡ Abelardo Margolles,§ Ruddy Wattiez,|| Hendrik W. van Veen,⊥ Wil N. Konings,§ Jean-Marie Ruysschaert,‡ and Erik Goormaghtigh*,‡

Laboratory of Structure and Function of Biological Membranes (SFMB), Free University of Brussels, B-1050 Brussels, Belgium, Department of Microbiology, Groningen Biomolecular Sciences and Biotechnology Institute, University of Groningen, Nl-9751 NN Haren, The Netherlands, Department of Pharmacology, University of Cambridge, Cambridge CB2 1QJ, United Kingdom, and Department of Biological Chemistry, University of Mons-Hainaut, B-7000 Mons, Belgium

Received January 3, 2001; Revised Manuscript Received June 19, 2001

ABSTRACT: Bacterial LmrA, an integral membrane protein of *Lactococcus lactis*, confers multidrug resistance by mediating active extrusion of a wide variety of structurally unrelated compounds. Similar to its eucaryotic homologue P-gp, this protein is a member of the ATP-binding cassette (ABC) superfamily. Different predictive models, based on hydropathy profiles, have been proposed to describe the structure of the ABC transporters in general and of LmrA in particular. We used polarized attenuated total reflection infrared spectroscopy, combined with limited proteolysis, to investigate the secondary structure and the orientation of the transmembrane segments of LmrA. We bring the first experimental evidence that the membrane-embedded domain of LmrA is composed of transmembrane-oriented α-helices. Furthermore, a new approach was developed in order to provide information about membrane domain dynamics. Monitoring the infrared linear dichroism spectra in the course of $^1H/^2H$ exchange allowed to focus the recording of exchange rates on the membrane-embedded region of the protein only. This approach revealed an unusual structural dynamics, indicating high flexibility in this antibiotic binding and transport region.

Multidrug resistance is an increasingly growing clinical problem in the treatment of infectious diseases and cancer. Among the mechanisms responsible for this phenomenon is the active extrusion of a wide variety of structurally unrelated compounds by integral membrane proteins such as ABC[1] transporters and secondary transporters (*1*). The secondary transporters are the most represented in the bacterial kingdom. They extrude toxic compounds using a proton motive force (*2*). The ABC transporters use the energy of ATP hydrolysis.

P-gp, a eucaryotic multidrug resistance protein, is the most studied ABC transporter (*3*). This protein is often implicated in resistance to chemotherapeutic compounds. Recently, a bacterial homologue of this protein, LmrA, has been discovered (*4*, *5*). It is the first ABC multidrug resistance transporter that has been discovered in bacteria. This protein can extrude different drugs out of the cell including compounds from different classes of antibiotics and antitumoral drugs (*5*, *6*). Thus, LmrA seems to be a good model for the study of multidrug resistance in antibiotic treatments as well as in chemotherapy. Presently, different topology models have been proposed on the basis of hydropathy profiles and sequence alignments (*4, 7*). The most commonly accepted ones suggest that these proteins are constituted of two homologous halves composed of an ATP-binding domain and a membrane-embedded domain (*8*). LmrA contains only one copy of each domain and seems to function in a dimeric form (*9*). Different experiments on P-gp suggest that the membrane-embedded domain is responsible for the recognition of the amphipathic substrates (*10*−*12*). Recent experiments on LmrA support the idea of two different binding sites (*9*). The first one, of high affinity, binds the antibiotics in the cytoplasmic leaflet of the membrane. Then, hydrolysis of ATP by the cytoplasmic domain brings the substrates to the low-affinity binding site on the external leaflet of the membrane, before releasing them into the aqueous phase (*13*). The coupling between the two domains may be induced by a change of conformation of the membrane domain or of the linker between the two domains (*14*).

Therefore, characterizing the structure of the membrane-embedded domain of LmrA is of major importance for the understanding of its molecular mechanism. Yet, a general picture of the structure and dynamics of the membrane-embedded domain of the protein is still missing. Present

† V.G. and C.V. are research fellows of the National Fund for Scientific Research (Belgium). A.M. is a recipient of a TMR fellowship of the EU. E.G. is Research Director of the National Fund for Scientific Research (Belgium).

* To whom correspondence should be addressed at the Free University of Brussels, Campus Plaine CP 206/2, B1050 Brussels, Belgium. Tel: (32) 2 6505386. Fax: (32) 2 6505382. E-mail: egoor@ulb.ac.be.

‡ Free University of Brussels.

§ University of Groningen.

|| University of Mons-Hainaut.

⊥ University of Cambridge.

[1] Abbreviations: ABC, ATP-binding cassette; ATR, attenuated total reflection; DDM, dodecyl β-D-maltoside; FTIR, Fourier transform infrared spectroscopy; IRE, internal reflection element; MDR, multidrug resistance; Ni−NTA, Ni^{2+}−nitrilotriacetic acid; PMSF, phenylmethanesulfonyl fluoride; PVDF, poly(vinylidene difluoride); SDS−PAGE, sodium dodecyl sulfate−polyacrylamide gel electrophoresis.

10.1021/bi010017+ CCC: $20.00 © 2001 American Chemical Society
Published on Web 09/08/2001

models suggest that the membrane-embedded domain is constituted of six α-helices (*4*) and that dimerization of two transmembrane domains allows the formation of a 12-helix translocation path. Spectroscopic studies (*14*, *15*) of other ABC transporters corroborate but do not confirm this model. Structural studies of synthetic CFTR transmembrane peptides show also an α-helix arrangement (*16*). Nevertheless, this does not constitute a proof of the α-helical nature of the entire membrane-embedded domain in its native conformation. An alternative model has been proposed for P-gp, suggesting that the membrane-embedded domain would adopt a *β*-sheet structure (*17*). Polarized attenuated total internal reflection infrared spectroscopy is presently one of the best tools available to gain information on the orientation of membrane-embedded peptides and protein secondary structures (*18, 19*). The method is simple, sensitive [less than 1 *μ*g of peptide is required (*20*)], and does not require specific labeling [although specific labeling with ^{13}C allows the study of selected residues (*21*)]. The use of this method, combined with limited proteolysis, allowed us to provide the first evidence for the presence of α-helices in the membrane-embedded domain of LmrA. It also demonstrates the perpendicular orientation of the helices with respect to the membrane plane. Furthermore, infrared spectroscopy provides insight in protein dynamics through the recording of $^1H/^2H$ exchange kinetics (*14, 22*−*24*). We combine here the use of polarized light and $^1H/^2H$ exchange kinetics to study specifically the stability of the membrane-embedded domain of LmrA.

EXPERIMENTAL PROCEDURES

Materials

D_2O was from Merck, Ni−NTA resin was from Qiagen, Bio-Beads SM2 were from Bio-Rad, polycarbonate filters were from Avestin, and DDM was from Anatrace. *Esccherichia coli* lipids and L-α-phosphatidylcholine from egg yolk were purchased from Avanti Polar Lipids. Proteinase K was from Sigma and PMSF from Serva. All sequencing reagents were from Beckman. Homemade softwares necessary for the analysis of infrared spectra were written in Matlab (The Mathworks).

Methods

Purification. The purification of LmrA was carried out essentially as described previously (*25*). Inside-out membrane vesicles, containing overexpressed LmrA, were solubilized in 50 mM potassium phosphate, pH 8, containing 10% (v/v) glycerol, 100 mM NaCl, and 1% (w/v) DDM. After 30 min of incubation at 4 °C, the insoluble material was removed by centrifugation. The supernatant was mixed and incubated for 1 h, at 4 °C, with Ni−NTA−agarose (≈8 mg of LmrA/mL of resin) which was preequilibrated in buffer A (50 mM potassium phosphate, 100 mM NaCl, 10% glycerol, and 0.05% DDM) (pH 8) plus 10 mM imidazole. The resin was transferred to a Bio-Spin column (Bio-Rad) and washed with 20 column volumes of buffer A containing 10 mM imidazole and subsequently with 40 column volumes of buffer A (pH 7) plus 40 mM imidazole. The protein was eluted with buffer A, pH 7, supplemented with 150 mM imidazole.

Reconstitution. Liposomes of acetone/ether-washed *E. coli* lipids and L-α-phosphatidylcholine from egg yolk, in a ratio (w/w) of 3:1, were made by dissolving lipids in 50 mM potassium phosphate, pH 7, at a final concentration of 20 mg/mL. Unilamellar liposomes with relatively homogeneous size were prepared by freezing in liquid nitrogen and slow thawing at room temperature, followed by extrusion of the liposomes 12 times through a 400 nm polycarbonate filter. The reconstitution of LmrA into liposomes was carried out essentially as described (*25*), using a protein:lipid ratio of 1:10 (w/w). The resulting proteoliposomes exhibited ATP-dependent drug transport and inhibition by chemosensitizers (*25*). Proteoliposomes were resuspended at a final protein concentration of 1 mg/mL in 3 mM potassium Hepes, pH 7.4.

Attenuated Total Reflection Fourier Transform Infrared Spectroscopy (ATR-FTIR). ATR-FTIR spectra were recorded, at room temperature, on a Bruker IFS55 FTIR spectrophotometer equipped with a liquid nitrogen-cooled mercury−cadmium−telluride (MCT) detector at a nominal resolution of 2 cm^{-1} and encoded every 1 cm^{-1}. The internal reflection element (IRE) was a germanium plate (50 × 20 × 2 mm) with an aperture angle of 45°, yielding 25 internal reflections (*26*). The spectrophotometer was continuously purged with air dried on a FTIR purge gas generator 75-62 Balston (Maidstone, England) at a flow rate of 5.8 L/min.

(A) Sample Preparation. Thin films of oriented multilayers were obtained by slowly evaporating the sample on one side of the ATR plate, under a stream of nitrogen (*27*). The ATR plate was then sealed in a universal sample holder. The sample contained 20 *μ*g of reconstituted LmrA.

(B) Secondary Structure Determination. The sample on the ATR plate was rehydrated by flushing ^2H_2O-satured N_2 for 2 h at room temperature. A total of 512 scans were averaged for each measurement. Secondary structure determination was based on the shape of the amide I band (1600−1700 cm^{-1}), which is sensitive to the secondary structure (*28*). The analysis was performed on the amide I region of deuterated samples because the $^1H/^2H$ exchange allows differentiation of the α-helical secondary structure from the random secondary structure whose absorption band shifts from about 1655 cm^{-1} to about 1642 cm^{-1} (*29*). Fourier self-deconvolution was applied to narrow the different components of the amide I region. Self-deconvolution was carried out using a Lorentzian line shape for the deconvolution and a Gaussian line shape for the apodization (*28*). To quantify the area of the different components of amide I revealed by self-deconvolution, a least squares iterative curve fitting was performed to fit Lorentzian line shapes to the spectrum between 1700 and 1600 cm^{-1} (*30*). To avoid the introduction of artifacts due to the self-deconvolution procedure, the fitting was then performed on the undeconvoluted spectrum. The proportion of a particular structure was computed as the sum of the area of all the fitted Lorentzian bands having their maximum in the frequency region where that structure occurs divided by the total area of the amide I. The frequency limits for each structure were assigned according to theoretical (*31*) or experimental (*32*) data: 1662−1645 cm^{-1}, α-helix; 1689−1682 and 1637−1613 cm^{-1}, *β*-sheet; 1644.5−1637 cm^{-1}, random; 1682−1662.5 cm^{-1}, *β*-turns (*28*).

(C) Orientation of the Secondary Structures. The molecular orientations by infrared ATR spectroscopy were determined

as previously described (*18*). Spectra were recorded with the incident light polarized parallel and perpendicular with respect to the incidence plane. Dichroism spectra were computed by subtracting the perpendicular polarized spectrum from the parallel polarized spectrum. The subtraction coefficient was chosen so that the area of the lipid ester band at 1740 cm^{-1} equals zero on the dichroism spectrum, to take into account the difference in the relative power of the evanescent field for each polarization as described before (*33*).

An upward deviation on the dichroism spectrum indicates a dipole oriented preferentially near a normal to the ATR plate. Conversely, a downward deviation on the dichroism spectrum indicates a dipole oriented closer to the plane of the ATR plate (*26*). The dichroic ratio R^{ATR} is defined as the ratio of the amide I area recorded for the parallel polarization ($A^{||}$) and perpendicular polarization ($A^{\perp}$):

$$R^{ATR} = A^{||}/A^{\perp}$$

In ATR, the dichroic ratio for an isotropic sample R^{iso} is different from unity and is computed on the basis of the area of the lipid ester band (1762−1700 cm^{-1}). As described previously, the presence in the sample of a fraction x of oriented helices and a fraction $1 - x$ of randomly oriented dipoles results in an experimental dichroic ratio R^{ATR} whose value lays between the value of the oriented helices dichroic ratio R^{α} and of the randomly oriented dipoles R^{iso}. Determination of R^{α} from x, R^{iso}, and R^{ATR} can be obtained from (*26*)

$$R^{\alpha} = A_{\alpha}^{||}/A_{\alpha}^{\perp} = \frac{R^{ATR} - \frac{R^{ATR}+2}{2R^{iso}+1}(1-x)}{1 - \frac{1}{R^{iso}}\frac{R^{ATR}+2}{2R^{iso}+1}(1-x)}$$

In the α-helical structure, the amide I dipole is oriented between 27° and 38° (*34*) with respect to the helix axis (for a review, see ref *35*). The mean orientation of the helix axis with respect to the membrane plane was estimated as described before (for a review, see ref *18*).

(D) Kinetics of Deuteration of the Whole Protein. Films containing 20 μg of reconstituted LmrA were prepared on a germanium plate as described above. Nitrogen was saturated with ^2H_2O by bubbling in a series of three vials containing ^2H_2O. Before starting the deuteration, 10 spectra of the sample were recorded to test the stability of the measurements. At zero time, the ^2H_2O-saturated N_2 flux, at a flow rate of 100 mL/min (controlled by a Brooks flow meter), was connected to the sample. For each kinetic time point, 24 scans were recorded and averaged at a resolution of 4 cm^{-1}. All of the spectra of the kinetics were corrected for atmospheric water absorption and side chain contribution. The subtraction of atmospheric water was done automatically by a home-written software which computed the subtraction coefficient as the ratio of the atmospheric water band between 1579 and 1572 cm^{-1} on the sample spectrum and on a reference atmospheric water spectrum (*36*, *37*). The contribution of the amino acid side chains was computed as a function of the extent of deuteration as previously described (*37*). This was done using the published contributions of the side chains in their protonated (*38*) and deuterated (*39*) forms. These data were recently reviewed (*35*, *40*). The area of amide II, characteristic of the δ(N−H) vibration, was obtained by integration between 1596 and 1502 cm^{-1}. For each spectrum, the area of amide II was divided by the corresponding lipid ν(C═O) area to take into account small but significant variations of the overall spectral intensity due to swelling of the sample layer at the beginning of the deuteration (*29*, *41*). This ratio, expressed in percentage, was plotted versus deuteration time. The 100% value is defined by the amide II/lipid ratio obtained before deuteration. The 0% value corresponds to a zero absorption in the amide II region, observed for a full deuteration of the protein.

(E) Kinetics of Deuteration of the Oriented Segments of the Protein. Film preparation and deuteration were carried out as described above except that parallel and perpendicular polarization spectra were recorded sequentially instead of a simple unpolarized spectrum for each time point. Before starting the deuteration, four spectra of the sample were recorded for each polarization. For each kinetic time point, 24 scans were recorded and averaged at a resolution of 2 cm^{-1} for each polarization. All of the spectra of the kinetics were corrected for atmospheric water absorption as described above.

Proteolysis of LmrA. Proteoliposomes (1 mg of LmrA/mL) were incubated with proteinase K (4 mg/mL) [proteinase K:LmrA ratio of 1:5 (w/w)] at room temperature for increasing periods of time from 1 min to 1 h. In all cases the proteolytic digestion was stopped by addition of phenylmethylsulfonyl fluoride to a final concentration of 1 mM (*19*). The proteoliposomes were then diluted in 2 mM NaHepes and 0.6 M NaCl, pH 7.4, and centrifuged for 90 min at 42 000 rpm in order to eliminate soluble and electrostatically bound peptides. The pellet was finally resuspended in 2 mM NaHepes, pH 7.4. Samples corresponding to different times of incubation were analyzed by SDS−PAGE 15% (*42*) and stained with silver nitrate (*43*).

One hour incubation was carried out for samples used for sequencing and infrared spectroscopy. For sequencing, lipids were extracted by a chloroform−methanol extraction (*44*).

N-Terminal Amino Acid Microsequence Analysis. Fragments were separated by SDS−PAGE, 15%, and electroblotted on a PVDF membrane. The fragments were then stained with Coomassie blue. The spots on the PVDF membrane were excised, and the protein N-terminal amino acid sequence was determined at the picomole level by automated Edman degradation of 1 pmol of protein using a Beckman LF3400D protein−peptide microsequencer equipped with an on-line model 168 diode array detector (Beckman instruments) (*45*). Carboxylmethylcysteine eluted just after glutamic acid in the PTH chromatograms. All samples were sequenced using the standard Beckman sequencer procedure 4. For internal sequencing, samples were treated with CNBr in acidic conditions (chemical cleavage at methionine), and peptides were purified by capillary RP HPLC.

Amino acid comparisons were carried out using the FASTA or the TFASTA computer program of the Genetics Computer Group for screening protein or nucleic acid databases. The international databases were SWISS-PROT (release 34), PIR (release 50), Genpept, Genpeptnew, GenEMBL (release 53), GenBank (release 105), GenEMBLnew (release 53.+), and IMGT (release 97.06).

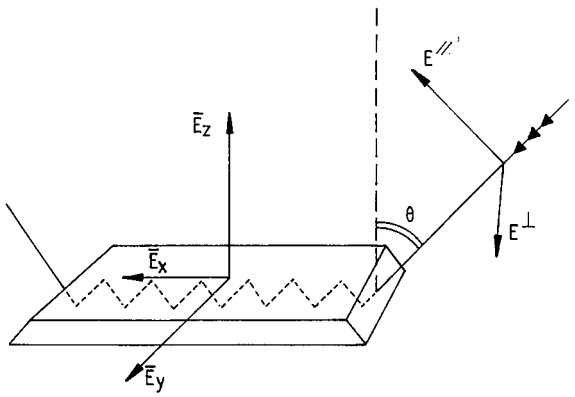

FIGURE 1: Schematic representation of the internal reflection element (IRE) and of the light pathway. The Cartesian components of the electric field are shown along the *X*, *Y*, and *Z* axes. Two possible planes of polarization of the incident light are indicated by $E_{||}$ (polarization parallel to the incidence plane) and $E_{\perp}$ (polarization perpendicular to the incidence plane). The incident beam makes an angle θ with respect to the normal to the IRE surface. The edges of the IRE are beveled so that the incident beam penetrates the IRE through a surface that is perpendicular to its propagation.

RESULTS

Orientations in LmrA. Polarized spectra recorded with the electric field vector of the IR radiation polarized parallel ($A^{||}$) or perpendicular ($A^{\perp}$) to the incidence plane appear in Figure 2. The lipid-associated $\nu_{as}(CH_2)$ and $\nu_s(CH_2)$ appear at 2918 and 2849 cm^{-1}, respectively (*27*). The lipid $\nu_{as}(CH_3)$ and $\nu_s(CH_3)$ are present at 2961 and 2873 cm^{-1}, respectively. Dichroism of these bands (see dichroic ratios below) reflects the orientation of the lipid acyl chains in the multilayer stack of lipid bilayers. A weak absorption at 3030 cm^{-1} can be assigned to $\nu(CH)_{\text{double bond}}$ and signs the presence of double bonds in the lipid acyl chains. The lipid intense band found between 1762 and 1705 cm^{-1} can be safely assigned to the lipid ester ν(C═O). Globally, the dichroism of this band is close to zero and can be used as a good approximation of a magic angle dichroism (*26*, *33*). It presents, however, a positive deviation at 1748 cm^{-1} and a negative deviation at 1729 cm^{-1}. The causes of these internal deviations have been investigated before. A major contribution of the lipids also appears at 1468 cm^{-1} and can be assigned to $\delta(CH_2)$.

Two important protein bands are found in the spectral window that exists between 1700 and 1500 cm^{-1}. Amide I (1700−1600 cm^{-1}) is the most intense absorption band of the polypeptides. Amide ν(C═O) has a predominant role in amide I. It accounts for 70−85% of the potential energy. ν(C−N) follows with 10−20% of the potential energy, and the C−CN deformation may account for about 10% of the potential energy. Amide I also contains some in plane NH bending, which is mainly responsible for the downshifts in the amide I frequency on N-deuteration (*31*). Amide I shape is conformational sensitive and generally used for secondary structure determination (for a review, see refs *30* and *46*). It shifts toward shorter wavenumbers by 2−10 cm^{-1} upon ^{1}H/^{2}H exchange (*30*). Amide II occurs in the 1580−1510 cm^{-1} region. It mainly derives from the in-plane N−H bending (40−60% of the potential energy). The rest of the potential energy arises from ν(C−N) (18−40%) and ν(C−C) (∼10%). Upon ^{1}H/^{2}H exchange, the in-plane N−^{2}H bending appears in the 1040−940 cm^{-1} region, and the ν(C−N) moves in the 1450−1490 cm^{-1} region where it mixes with other modes to yield a new band called amide II′. Analysis of nondichroic amide I shape reveals the secondary structure of the protein: α-helix, 35%; β-sheet, 24%; turns, 28%; unordered, 14% (*14*). Amide I displays a strong positive dichroism with a maximum at 1659 cm^{-1} (Figure 2), indicating that (1) the oriented structure is essentially helical in nature since the maximum of the dichroism is characteristic of α-helix structure and (2) the helices are oriented mainly perpendicular to the IRE surface, i.e., perpendicular to the membrane plane.

Quantitative evaluation of the helix mean tilt requires the evaluation of the dichroic ratio $R^{ATR} = A^{||}/A^{\perp}$ for amide I and of R^{iso}, which is the dichroic ratio measured for a transition dipole either spatially disordered or oriented at the magic angle (*26*, *33*). As indicated above and developed in detail elsewhere (*33*), the lipid ν(C═O) was used to determine R^{iso}. For the example presented on Figure 2, $R^{iso} = 1.5$. The perpendicular orientation of the lipid acyl chains with respect to the IRE surface is demonstrated by $R^{ATR} = 1.9$ for $\nu_{as}(CH_3)$ and $R^{ATR} = 1.4$ for $\nu_s(CH_2)$, i.e., respectively above and below R^{iso}. As $R^{ATR} = 1.9$ for amide I, it confirms that the preferred orientation of the protein helices is perpendicular to the membrane. Quantitative results will be discussed later. Yet, it remains to be determined whether these oriented helices are part of the membrane-embedded domain of the protein or are located in its cytoplasmic domain. The fact that the dichroism of amide II is also positive could suggest that the R^{iso} value is not large enough. In fact, it is possible to select a scaling coefficient (which turns out to be close to the one used here) that would leave amide I dichroism positive and amide II dichroism negative as expected. The decisive advantage of the procedure we have been following here is that it allows us to take into account the film thickness. Considering that R^{iso} values range between 1.1 for the thin film hypothesis and 2.0 for the thick film hypothesis, it is necessary to take this problem into account. Comparison of IR dichroism data using the ester ν(C═O) band to determine R^{iso} with solid-state NMR data indicated that the approximation is good for quantitative analyses as demonstrated earlier (*33*). The fact that we obtain only an approximation of R^{iso} is obvious, but this approximation has been shown to be good enough to establish the orientation of various peptides in films of different thicknesses and will be used in the present work.

Proteolysis of LmrA. To isolate the membrane-embedded domain of LmrA, proteoliposomes were treated with proteinase K (see Experimental Procedures). With this procedure, we potentially removed the cytoplasmic domain of LmrA, leaving intact the membranous and vesicle interior parts of the protein. Proteinase K was added to the LmrA-containing proteoliposomes in a 1:5 (w/w) protein ratio for 1, 5, 15, and 30 min in order to remove the cytoplasmic domain of the protein. Figure 3 indicates a fast cleavage of the protein as no band of the intact protein (65 kDa) is observed after the beginning of the proteolysis. Among the peptides generated by proteolysis, the one at 35 kDa apparent molecular mass is stable (for at least 6 h; result not shown) and remains the main species present after 15 min. To eliminate a maximum of the other peptides generated by proteolysis, we selected an incubation time of 1 h for the samples used for further analysis. Centrifugation of the sample was carried out to eliminate any peptide not associ-

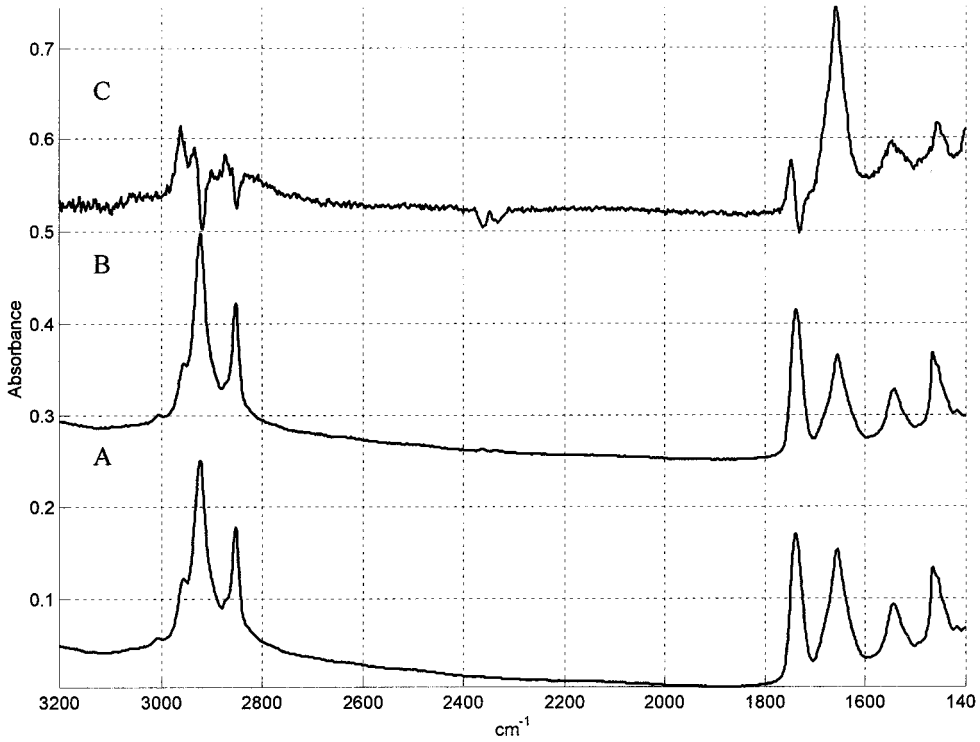

FIGURE 2: Polarized infrared and dichroism spectra of LmrA. ATR-FTIR spectra of 20 μg of LmrA recorded with incident light polarized parallel (A) or perpendicular (B) to the incidence plane. The dichroism spectrum (C) is obtained by subtraction of the perpendicular polarized spectrum from the parallel polarized one as described in Experimental Procedures. The *Y* scale is given in reference to spectrum A; spectra B and C were offset for clarity. The difference spectrum *C* scale has been increased 4-fold.

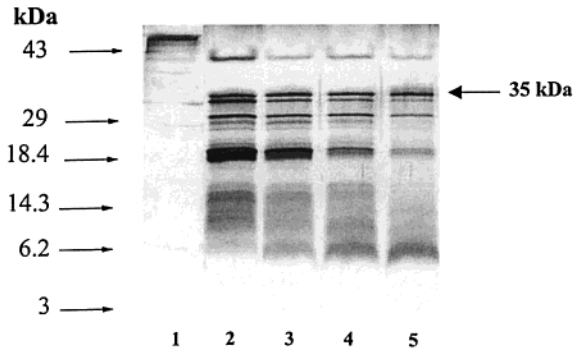

FIGURE 3: Gel electrophoresis after proteolysis of LmrA by proteinase K. LmrA was proteolyzed with proteinase K in a 5:1 (w/w) ratio. Each lane contains 8 μg of LmrA, before proteolysis (lane 1) or proteolyzed during 1 (lane 2), 5 (lane 3), 15 (lane 4), and 30 (lane 5) min. The band present at 40 kDa is due to the presence of ethanol in the sample and is not observable after the centrifugation step.

ated with the lipids. Gel electrophoresis of the pellet showed the same bands as before centrifugation, suggesting that cytoplasmic peptides are digested by proteinase K (results not shown). The 35 kDa peptide was then blotted on a PVDF membrane and sequenced as explained in Experimental Procedures. Because it was blocked at the N-terminus, the peptide was submitted to CNBr cleavage. The following sequence was then obtained: VQPLINSFGHGV corresponding to the sequence of the protein starting after M^{58} (*4*). Because of its size, the 35 kDa peptide is therefore expected to encompass just the six transmembrane helices and the loop connecting them according to the protein predicted model. Since the other minor peptides visible on the gel are membrane bound and resistant to proteolysis, they might be smaller fragments of the 35 kDa peptide cut in the loops that connect the transmembrane segments.

Orientation in the Membrane Peptide of LmrA. Infrared spectra of the proteolyzed sample were recorded as described for the intact protein (spectra not shown). Analysis of amide I shape, in Figure 4, reveals that the α-helix content of the protein rises from 35% in the intact protein to 65% in the membrane-bound peptides left after proteinase K treatment. Furthermore, only 7% of β-sheet structure was found for the cleaved sample. Nevertheless, it has to be stressed that these percentages are not absolute values because of the presence of the smaller fragments associated with the membrane, although the duration of the proteolysis step has been chosen in order to minimize their effect. Dichroism analysis (not shown) yields $R^{iso} = 1.5$ and $R^{ATR} = 2.4$ for amide I. Again, the frequency of the dichroism maximum (1656 cm^{-1}) indicates that it arises from helical structures. If we assume that all of the helices present in the proteolyzed sample are transmembrane helices and that the remaining structures (mainly loops) display no preferential spatial orientation of their amide C═O groups, then, using the equation described in Experimental Procedures (*47*), it comes that $R^{\alpha} = 2.7$ (with $R^{iso} = 1.5$ and $R^{ATR} = 2.4$). Similarly, assuming that the only oriented structures are the transmembrane helices (20% of the amino acid residues according to the six transmembrane segment model) in the intact protein ($R^{iso} = 1.5$ and $R^{ATR} = 1.9$), it comes that $R^{\alpha} = 2.6$. The nonsignificant difference between the R^{α} values estimated for the entire protein and for the membrane-bound proteolytic peptides indicates that all of the dichroism present in the intact protein can be explained by the dichroism associated with the membrane-embedded helices. The mean orientation of the helices obtained from the dichroic ratios is evaluated

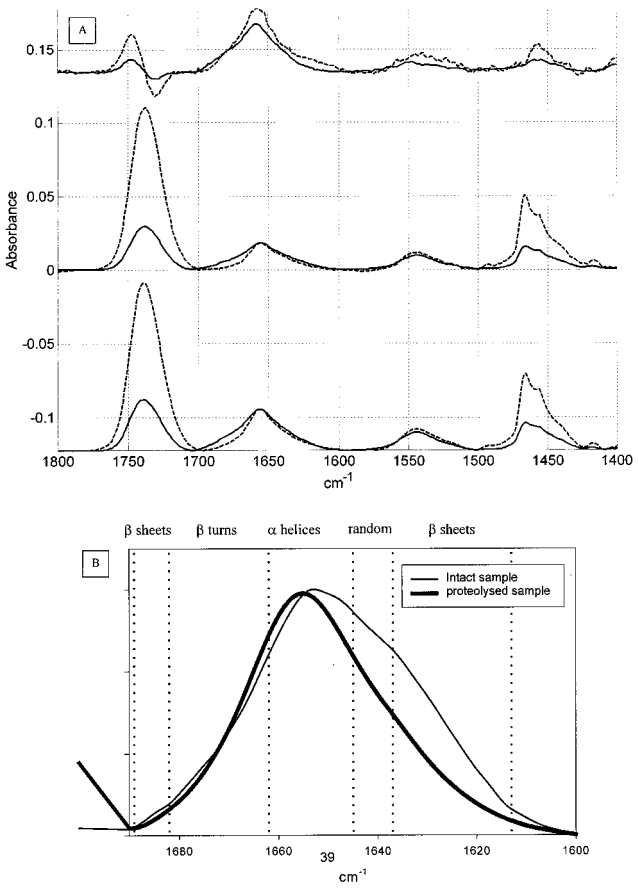

FIGURE 4: ATR-FTIR spectra of the intact and cleaved samples. (A) Polarized and dichroic spectra of the intact (solid line) and proteolyzed (dashed line) samples. From the bottom to the top: parallel polarization, perpendicular polarization, and dichroic spectra. (B) Spectra of the deuterated intact (thin line) and proteolyzed (thick line) sample.

between 18° and 35° with respect to the IRE normal, depending on the orientation of the amide I dipole [from 27° to 38° (*34*, *35*)]. Such a tilt is found for most of the transmembrane segments in membrane proteins.

LmrA Stability−^{1}H/^{2}H Exchange Kinetics. At constant pH and temperature, the rate of amide hydrogen exchange by deuterium is related to the stability of the secondary structures and to the solvent accessibility to the NH amide groups. In Figure 5, a series of spectra recorded as a function of the deuteration time is reported. Upon deuteration, there is a limited shift in the amide I region, a decrease of the amide II intensity near 1550 cm^{-1}, and an increase of the amide II′ intensity near 1450 cm^{-1}. Amide hydrogen exchange was followed by monitoring the amide II absorption peak decrease as a function of the time of exposure to ^2H_2O-saturated N_2 flow (from 10 s to 240 min; for details, see Experimental Procedures). Integration of lipid ν(C═O) and amide II bands was performed using the baselines drawn on the figure. The decreasing area of amide II computed between 0 and 100% (see Experimental Procedures) is reported in Figure 6. Further insight into the process was obtained considering that the hydrogen/deuterium exchange is the sum of first-order reactions. The fraction of unexchanged amide protons $H(t)$ can therefore be described as a sum of individual exponentials. Practically, considering only a few classes of exchange rates (three classes in the present case) allows the description of the data within the experimental error limits (*23*). Each exponential corresponds then to a group, i, of amide bonds characterized by a common time constant, T_i:

$$H(t) = \sum_i a_i \exp(-t/T_i)$$

where a_i is the proportion of residues belonging to group i. For three populations of amide protons ($i = 1, 2, 3$), least squares curve fitting yields three time constants $T_{1,2,3}$ and three proportions $a_{1,2,3}$. We found $T_1 = 0.2$ min, 31%, $T_2 =$ 2 min, 15%, and $T_3 = 500$ min, 54%.

LmrA Membrane Domain Stability−^{1}H/^{2}H Exchange Kinetics. While the global exchange kinetics of the protein can be evaluated from the amide II area decrease as a function of time, amide I experiences only limited shifts (5−15 cm^{-1}) (*30*). Even though the relation between the frequencies of the different components of amide I and secondary structures is better established (for a review, see refs *30* and *46*), the component large width at half-height and the comparatively small shifts upon deuteration make these shifts difficult to investigate in terms of secondary structure (*48*, *49*). In the present case, however, the experiments carried out above suggest that the dichroism spectrum (Figure 2, spectrum C) arises only from the oriented helices embedded in the membrane. As the amide II presents no strong dichroism property, we may not use it to monitor the ^{1}H/^{2}H exchange. On the other hand, the shift of the amide I dichroism spectrum can provide us with the necessary tool to evaluate specifically the exchange rate of the transmembrane helices. The advantage of this approach resides in the possibility of monitoring the oriented transmembrane helices only, ignoring the rest of the protein which does not contribute to the dichroism spectrum. For this purpose a series of polarized spectra were recorded in the course of the exchange process. Dichroism spectra were generated as explained in Figure 2. A time series of such dichroism spectra appears in Figure 7. To monitor quantitatively the exchange process, we fitted the amide I dichroism peak as the combination of two Lorentzian/Gaussian (Cauchy functions) bands. The first one at higher frequency would represent the ^{1}H form of the helices and is expected to decrease in the course of the exchange process. The second one at lower frequency would represent the ^{2}H form of the helices and is expected to increase in the course of the exchange process. A first unconstrained curve fitting carried out on the undeuterated sample and on a sample deuterated for 4 days (not shown) indicated that the frequency of the ^{1}H and ^{2}H contributions were 1658 and 1648 cm^{-1}, respectively. The width at half-height was found to be 25 and 30 cm^{-1}, respectively. These values were then used in a constrained curve fitting to analyze the time series presented in Figure 7. The intensity of the band at 1658 cm^{-1} was scaled between 100% and 0% and plotted in Figure 8. It appears, according to Figure 8, that after 20 min 60% of the oriented helix amide groups have been exchanged, i.e., an unexpected fast exchange for the transmembrane region of the protein. Furthermore, it is obvious that several distinct rate constants are necessary to describe the exchange curve reported in Figure 8. A decomposition of this exchange curve indicates that 48% of the amino acid residues belonging to the oriented membrane helices of the protein experience a very fast exchange (time constant 0.2 min). Conversely, another 37% seem almost inaccessible by solvent and do not experience

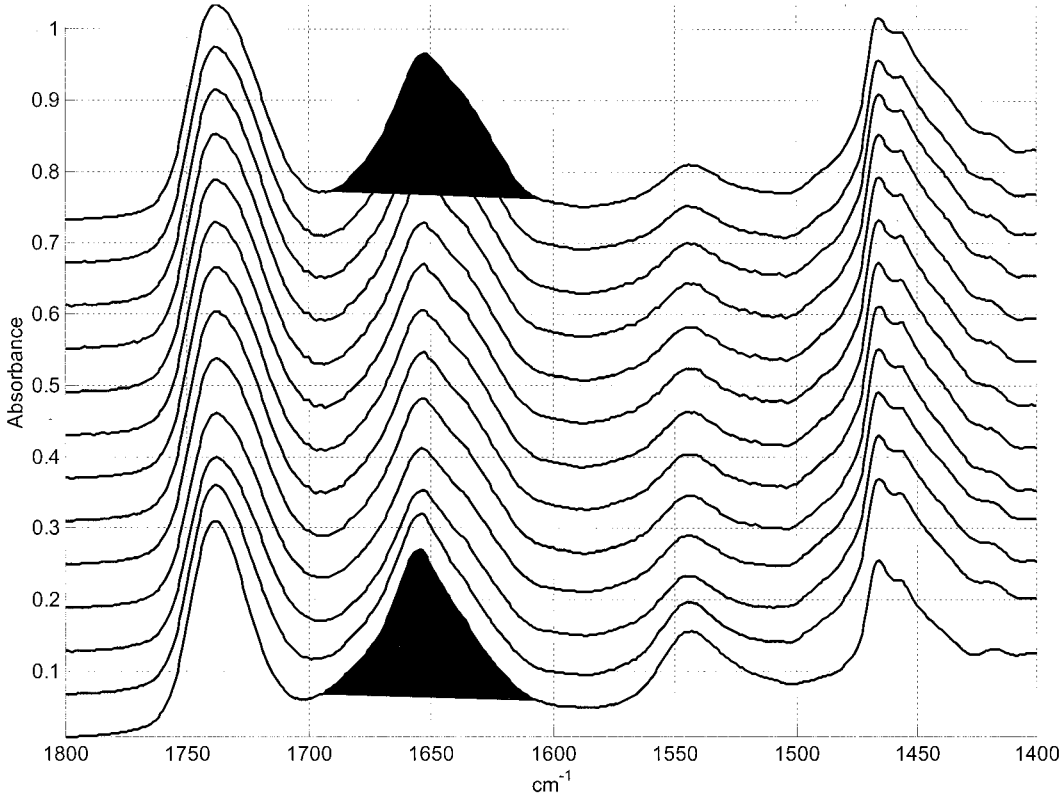

FIGURE 5: $^1H/^2H$ exchange kinetic spectra of LmrA. Spectra of 20 μg of LmrA recorded as a function of the deuteration time. The spectrum at the bottom has been recorded before deuteration and the one at the top after 3 h of deuteration. The other spectra have been recorded at intermediate times (1, 4, 7, 11, 14, 18, 21, 25, 29, 42, and 93 min, respectively). The *Y* scale is given in reference to the spectrum at the bottom; other spectra were offset for clarity.

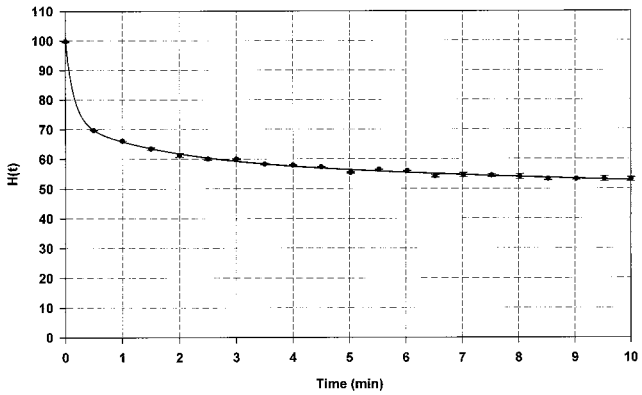

FIGURE 6: Exchange curve of LmrA. Evolution of the proportion of unexchanged amide bonds of LmrA [$H(t)$] computed between 0 and 100% presented as a function of the deuteration time. Only the first 10 min are shown. Error bars represent the standard deviation computed for four independent experiments. The full line was obtained by a fitting procedure of exponential decay.

any exchange (time constant 2000 min). To make sure that this analysis is robust, we checked the effect of varying the scaling factor used for generating the dichroic spectra. We increased the scaling factor by up to 25%. In these conditions, dichroism spectra obtained by subtracting the perpendicular polarized spectra from the parallel polarized spectra displayed a positive deviation in the amide I frequency range and a negative deviation in the amide II frequency range (not shown). Yet, analysis of the exchange curve performed as described above revealed that the proportion of the fast exchanging component was stable within 2% (results not shown).

DISCUSSION

Due to the presence of lipids, information about the structure of integral membrane proteins remains difficult to obtain. For most of the membranous proteins, the only structural information relies upon predictive models based on hydropathy profiles and sequence alignments. For ABC transporters, the crystal structure of HisP, the ATP-binding subunit of a histidine transporter of *E. coli*, has brought information about the structure of the nucleotide binding domain (*50*). For the entire transporter, the most precise structure is the one determined for P-gp by electron microscopy with a resolution of 2.5 nm (*51*). However, it provides no information about the secondary structure and organization of the peptide chains within each domain. Because the membrane-embedded domain seems to be essential in the recognition and transport of substrates (*10*−*12*), characterizing the structure of this domain in LmrA remains necessary.

ABC transporters are made of two homologous halves composed of a nucleotide binding domain and a transmembrane domain. Although a β-sheet model has been proposed (*17*), the most accepted theoretical model of LmrA and other ABC transporters suggests that the transmembrane segments are helical (*4*, *8*). To confirm experimentally this model, we have, in a first step, demonstrated the presence in LmrA of α-helices oriented perpendicularly to the membrane plane. The membrane-embedded domain of LmrA was then isolated after digestion of reconstituted LmrA by proteinase K. This produced a fragment that has been shown to include the six predicted transmembrane segments and the loops connecting

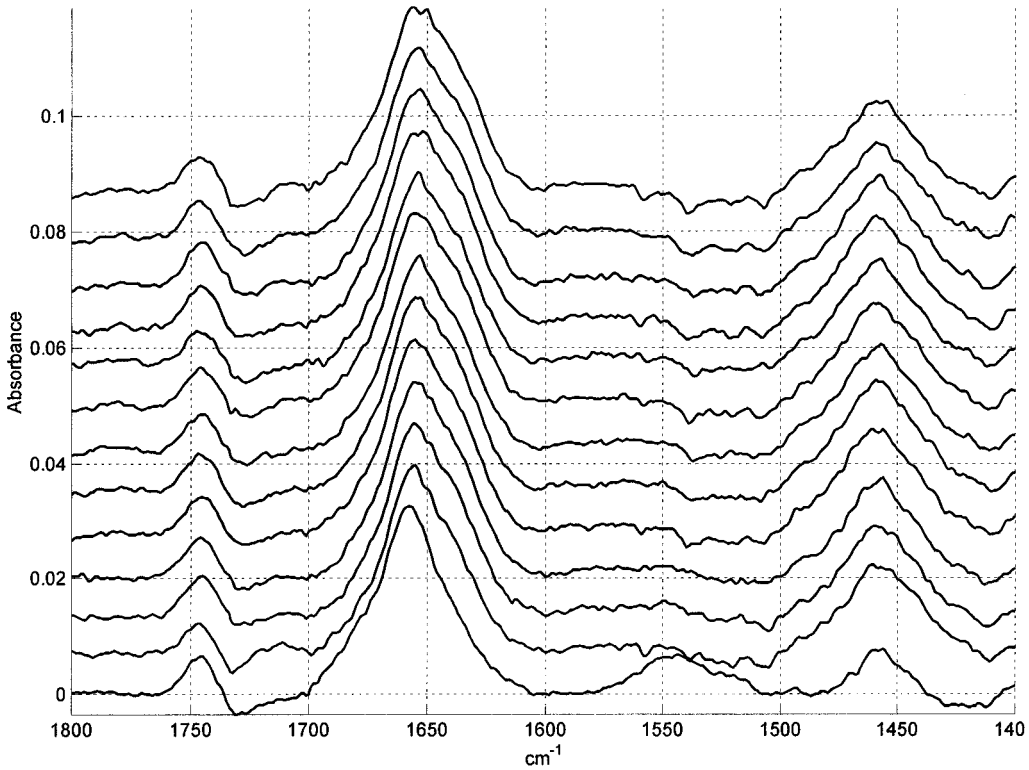

FIGURE 7: Dichroic spectra of intact LmrA recorded in the course of $^1H/^2H$ exchange. Polarized spectra of 20 μg of LmrA were recorded as a function of deuteration time, and dichroism spectra were obtained as described in Figure 2. The dichroism spectrum at the bottom has been recorded before deuteration and the one at the top after 3 h of deuteration. The other spectra have been recorded at intermediate times (1, 4, 7, 11, 14, 18, 21, 25, 29, 42, and 93 min, respectively). The *Y* scale is given in reference to the spectrum at the bottom; other spectra were offset for clarity.

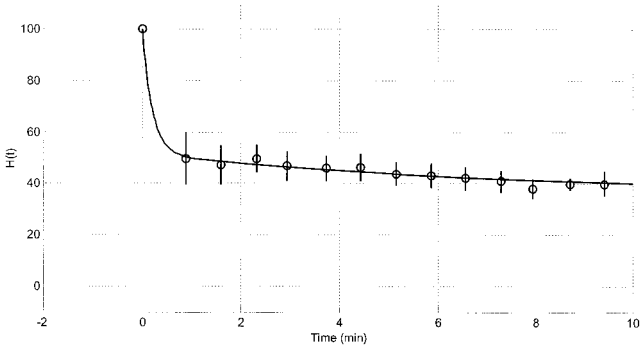

FIGURE 8: Exchange curve of transmembrane domains of LmrA. Evolution of the proportion of exchanged amide bonds of transmembrane segments of LmrA computed between 0 and 100% is presented as a function of the deuteration time. Only the first 10 min are shown. Error bars represent the standard deviation computed for four independent experiments. The full line was obtained by a fitting procedure of exponential decay.

them. The ATR-FTIR spectrum of the proteolyzed sample demonstrated that the membrane-embedded domain of LmrA is indeed helical. Furthermore, the small quantity of β-sheet structure found in the cleaved sample strongly suggests the absence of a transmembrane β-barrel, at least for LmrA. This is the first direct experimental evidence of the helical nature of the transmembrane segments for an ABC transporter. The homology of LmrA with P-gp mainly, but also with the other ABC transporters, suggests that this may be a common feature for most proteins of this superfamily. Furthermore, infrared dichroism confirmed the perpendicular orientation of these helices with respect to the membrane plane.

Interestingly, the entire dichroism contained in the protein arises from helical structures, suggesting that no other secondary structure has, on the average, a specific orientation with respect to the membrane. Even more interesting is the fact that the dichroism present in the intact protein can be completely explained by the dichroism of the helices which remain associated with the membrane after proteinase K treatment. This observation strongly suggests that only the transmembrane helices contribute significantly to the dichroism. If we accept this hypothesis, it makes it possible to monitor the $^1H/^2H$ exchange rate of the transmembrane domain only while working with the intact protein. However, the possibility that oriented segments in the region of the protein that protrude from the membrane may have opposing dichroism and, consequentely, cancel each other should be considered. There would then be no net contribution to the dichroism before deuteration, but change in the dichroism could occur as a function of the exchange. We shall examine here three potential situations:

(1) Nonmembrane helical contribution: To obtain a significant effect we need to imagine that a number of conditions are fulfilled simultaneously:

Among the nonmembrane helices, only the ones with an orientation close to a parallel or a perpendicular to the membrane do contribute with a significant intensity to the dichroism spectrum.

Among the latter population of helices, it should happen that they form a pair with orientations normal with respect to each other, leading to no net dichroism.

The latter pair of helices should display exchange constants dramatically different.

Finally, all the fast-exchanging helices should be the ones perpendicular to the membrane in order to contribute to a fast, transiently uncompensated, intensity decrease at 1658 cm^{-1}.

As LmrA contains 35% of α-helices, considering 6 transmembrane helices of ca. 20 residues each, it comes that only 14% of the helices belong to nonmembrane parts of the protein. Simple computation indicates that only one-third of the observed fast-exchanging contribution at most could be explained if all of the conditions above are simultaneously fulfilled.

(2) Nonmembrane, nonhelical contributions: According to published assignments, only a "random coil" contribution could also be present at 1658 cm^{-1}. It has been shown before that random structures always undergo very fast exchange (*48*, *49*). Therefore, within a few seconds, all the coil contributions should reach the same state of full deuteration with no effect on the dichroism.

(3) Nonmembrane helical/coil contributions: Assuming that all of the hypotheses developed about the nonmembrane helical contribution are fulfilled, the possibility should be envisaged. To rule out this possibility, we recorded the evolution of dichroic spectra on the digested protein. In this new situation, the large majority of the nonmembrane helices and random coil structures have been removed by the proteolytic activity. The results clearly indicated that the oriented part of the membrane region of LmrA isolated after proteolysis also displays a fast component (data not shown).

In conclusion, we think that we can rule out the possibility that the fast-exchanging fraction of amino acid residues detected in the polarized experiments can be assigned to nonmembrane residues. In turn, the fact that the dichroism present in the intact protein can be completely explained by the dichroism of the helices which remain associated with the membrane after proteinase K treatment strongly suggests that only the transmembrane helices contribute significantly to the dichroism. If we accept this hypothesis, it makes it possible to monitor the $^1H/^2H$ exchange rate of the transmembrane domain only while working with the intact protein.

The rate of exchange of protein hydrogens is one way to approach a description of structure fluctuations. $^1H/^2H$ exchange rate measurements yield information not available from equilibrium methods. In ATR-FTIR spectroscopy experiments, the exchange rate is similar to the one found in solution (*52*, *53*). Furthermore, after resuspension of the film of LmrA in 2 mM Hepes, pH 7.4, no loss of ATPase activity was observed (not shown), confirming that film preparation does not alter the protein conformation and activity. Secondary structures stabilized by hydrogen bonds are resistant to exchange to an extent that depends on their stability. Furthermore, burial of peptide groups in the hydrophobic region of the folded protein prevents the access of the solvent required for the exchange and stabilizes the secondary structure. Helix−helix interactions have also been shown to modulate the exchange rate (*54*).

Numerous examples indicate that the $^1H/^2H$ exchange of membrane-embedded helices from integral membrane proteins is extremely slow. Monitoring the exchange of bacteriorhodopsin between 1.5 and 25 h after addition of ^2H_2O was carried out by Downer et al. (*55*). The authors found a plateau reached after about 10 h where some 70% of the amide groups remain unexchanged (60% for rhodopsin). These values roughly correspond to the membrane-embedded helical fraction of the protein. They also agree with ATR data obtained on a film which show 80% of unexchanged amide after 2 h exposure to ^2H_2O and 73% unexchanged amide after 48 h exposure to ^2H_2O (*56*). Exchange kinetics for individual backbone amides has been found by NMR to present a periodicity in melittin reconstituted in bilayers (PC:PS 88:12 mol/mol) with an exchange rate 20-fold slower for the amino acids located on the hydrophobic face of the helix (*57*). Insertion of the transmembrane segment of glycophorin results in the presence of an amide population which is virtually unexchangeable (*58*, *59*). Similarly, stable α-helices from pulmonary surfactant SP-C (*60*, *61*) and SP-B (*62*) exchange very slowly. Conversely, some helices from integral membrane proteins display fast exchange rates. The human erythrocyte glucose exchanger exhibits a fast exchange rate (*63*): at p^2H 7, 81% of the amide groups are exchanged after 1 h in the presence of ^2H_2O. Very little exchange takes place during the following 3 days. Yet, a model of this protein proposes 12 α-helices crossing the membrane accounting for about 50% of the 492 amino acids of the protein. The lactose permease also displays an unusually fast exchange as shown by Le Coutre et al. (90−95% exchange completion) (*64*). Fast exchange rates have also been reported for the gastric H^+,K^+-ATPase (*47*). Finally, the water channel CHIP28 presents 80% of exchange within 5 min (*65*). Other membrane-interacting proteins display fast exchange. Binding of cytochrome *c* onto the negatively charged surface of DMPG or DOPG vesicles results in destabilization of the α-helices as indicated by differential scanning calorimetry and by the immediate and complete $^1H/^2H$ exchange recorded (*66*, *67*). A similar behavior is observed for apolipoproteins with amphipathic helices such as apolipophorin (*68*). Fast exchange is associated to either large protein structural fluctuations or to large accessibility of membrane-bound domains to the solvent. The present work reveals that the transmembrane helices of LmrA display a rate of exchange that is fast, implying that the transmembrane helical segments of LmrA are more flexible and accessible than most (but not all) of the transmembrane helical segments described so far in the literature. This could be related to the specific function of LmrA, which is to transport structurally unrelated amphipathic molecules across the membrane. Furthermore, experimental data on related proteins support this interpretation. Indeed, electron microscopy images of P-gp clearly show the presence of an aqueous chamber in the membrane (*51*). This chamber has an aperture of as much as 5 nm in diameter (compared to 0.3 nm for bacteriorhodopsin) on the external surface, allowing solvent accessibility in the membrane domain. Furthermore, cysteine cross-linking experiments on P-gp demonstrate that consecutive residues of helices 4 and 10 can be cross-linked with residues of helices 12 and 6, respectively (*69*). These data implicate the occurrence of large translational and rotational movements of the transmembrane helices. This high flexibility is in agreement with the high exchange rate observed. Therefore, we think that, although a high exchange rate in the membrane domain is exceptional, it is not so surprising when dealing with multidrug resistance proteins. We believe that the protein may function as a hydrophobic vacuum cleaner as suggested

by van Veen et al. (*9*, *13*). The substrates bind to the membrane and, after hydrolysis of ATP and concomitant change of conformation, are released at the level of an aqueous chamber connected to the extracytoplasmic space. Conversely, another fraction of the membrane-embedded domain of LmrA (37%) has a very low rate of exchange. They may represent the amino acids that are in direct contact with the lipid phase.

In conclusion, we present here the first experimental evidence of the structure and orientation of the membrane-embedded domain of LmrA or any ABC transporter. Furthermore, we designed a method which permitted us to investigate structural dynamics of the membrane part of the protein. This approach revealed an unusual structure dynamics in the membrane region of the protein which is to be related to the particular function of this protein domain. This new experimental approach is of general interest for the study of other membrane proteins. This possibility to specifically study the dynamics of the oriented domain of a protein without altering its integrity may bring information on the mechanism of numerous membranous processes.

REFERENCES

1. Nikaido, H. (1994) *Science 264*, 382−388.
2. Paulsen, I. T., Brown, M. H., and Skurray, R. A. (1996) *Microbiol. Rev. 60*, 575−608.
3. Gottesman, M. M., and Pastan, I. (1993) *Annu. Rev. Biochem. 62*, 385−427.
4. van Veen, H. W., Venema, K., Bolhuis, H., Oussenko, I., Kok, J., Poolman, B., Driessen, A. J., and Konings, W. N. (1996) *Proc. Natl. Acad. Sci. U.S.A. 93*, 10668−10672.
5. van Veen, H. W., Callaghan, R., Soceneantu, L., Sardini, A., Konings, W. N., and Higgins, C. F. (1998) *Nature 391*, 291−295.
6. Putman, M., van Veen, H. W., Degener, J. E., and Konings, W. N. (2000) *Mol. Microbiol. 36*, 772−773.
7. Jones, P. M., and George, A. M. (2000) *Eur. J. Biochem. 267*, 5298−5305.
8. Higgins, C. F. (1992) *Annu. Rev. Cell Biol. 8*, 67−113.
9. van Veen, H. W., Margolles, A., Muller, M., Higgins, C. F., and Konings, W. N. (2000) *EMBO J. 19*, 2503−2514.
10. Greenberger, L. M. (1993) *J. Biol. Chem. 268*, 11417−11425.
11. Loo, T. W., and Clarke, D. M. (1999) *J. Biol. Chem. 274*, 24759−24765.
12. Zhang, X., Collins, K. I., and Greenberger, L. M. (1995) *J. Biol. Chem. 270*, 5441−5448.
13. Bolhuis, H., van Veen, H. W., Molenaar, D., Poolman, B., Driessen, A. J., and Konings, W. N. (1996) *EMBO J. 15*, 4239−4245.
14. Vigano, C., Margolles, A., van Veen, H. W., Konings, W. N., and Ruysschaert, J. M. (2000) *J. Biol. Chem. 275*, 10962−10967.
15. Dong, M., Ladaviere, L., Penin, F., Deleage, G., and Baggetto, L. G. (1998) *Biochim. Biophys. Acta 1371*, 317−334.
16. Wigley, W. C., Vijayakumar, S., Jones, J. D., Slaughter, C., and Thomas, P. J. (1998) *Biochemistry 37*, 844−853.
17. Jones, P. M., and George, A. M. (1998) *J. Membr. Biol. 166*, 133−147.
18. Goormaghtigh, E., and Ruysschaert, J. M. (1990) in *Molecular Description of Biological Membranes by Computer Aided Conformational Analysis* (Brasseur, R., Ed.) pp 285−329, CRC Press, Boca Raton, FL.
19. Vigneron, L., Ruysschaert, J. M., and Goormaghtigh, E. (1995) *J. Biol. Chem. 270*, 17685−17696.
20. Demel, R. A., Goormaghtigh, E., and de Kruijff, B. (1990) *Biochim. Biophys. Acta 1027*, 155−162.
21. Ludlam, C. F., Arkin, I. T., Liu, X. M., Rothman, M. S., Rath, P., Aimoto, S., Smith, S. O., Engelman, D. M., and Rothschild, K. J. (1996) *Biophys. J. 70*, 1728−1736.
22. Sonveaux, N., Shapiro, A. B., Goormaghtigh, E., Ling, V., and Ruysschaert, J. M. (1996) *J. Biol. Chem. 271*, 24617−24624.
23. Goormaghtigh, E., Vigneron, L., Scarborough, G. A., and Ruysschaert, J. M. (1994) *J. Biol. Chem. 269*, 27409−27413.
24. Gregory, R. B., and Rosenberg, A. (1986) *Methods Enzymol. 131*, 448−508.
25. Margolles, A., Putman, M., van Veen, H. W., and Konings, W. N. (1999) *Biochemistry 38*, 16298−16306.
26. Goormaghtigh, E., Raussens, V., and Ruysschaert, J. M. (1999) *Biochim. Biophys. Acta 1422*, 105−185.
27. Fringeli, U. P., and Gunthard, H. H. (1981) *Mol. Biol. Biochem. Biophys. 31*, 270−332.
28. Goormaghtigh, E., Cabiaux, V., and Ruysschaert, J. M. (1990) *Eur. J. Biochem. 193*, 409−420.
29. Goormaghtigh, E., Cabiaux, V., and Ruysschaert, J. M. (1994) *Subcell. Biochem. 23*, 363−403.
30. Goormaghtigh, E., Cabiaux, V., and Ruysschaert, J. M. (1994) *Subcell. Biochem. 23*, 405−450.
31. Krimm, S., and Bandekar, J. (1986) *Adv. Protein Chem. 38*, 181−364.
32. Susi, H., and Byler, D. M. (1986) *Methods Enzymol. 130*, 290−311.
33. Bechinger, B., Ruysschaert, J. M., and Goormaghtigh, E. (1999) *Biophys. J. 76*, 552−563.
34. Marsh, D., Muller, M., and Schmitt, F. J. (2000) *Biophys. J. 78*, 2499−2510.
35. Goormaghtigh, E., Cabiaux, V., and Ruysschaert, J. M. (1994) *Subcell. Biochem. 23*, 329−362.
36. Goormaghtigh, E., and Ruysschaert, J. M. (1994) *Spectrochim. Acta 50*, 2137−2144.
37. Goormaghtigh, E., de Jongh, H. H., and Ruysschaert, J. M. (1996) *Appl. Spectrosc. 50*, 1519−1527.
38. Chirgadze, Y. N., Fedorov, O. V., and Trushina, N. P. (1975) *Biopolymers 14*, 679−694.
39. Venyaminov, S. Y., and Kalnin, N. N. (1990) *Biopolymers 30*, 1243−1257.
40. Barth, A. (2000) *Prog. Biophys. Mol. Biol. 74*, 141−173.
41. Harrick, N. J. (1967) in *Internal Reflection Spectroscopy*, Interscience Publishers, New York.
42. Laemmli, U. K. (1970) *Nature 227*, 680−685.
43. Merril, C. R., Goldman, D., and Van Keuren, M. L. (1983) *Methods Enzymol. 96*, 230−239.
44. Bligh, E. G., and Dyer, W. J. (1959) *Can. J. Biochem. Physiol. 37*, 911−917.
45. Bex, F., Murphy, K., Wattiez, R., Burny, A., and Gaynor, R. B. (1999) *J. Virol. 73*, 738−745.
46. Arrondo, J. L., Etxabe, I., Dornberger, U., and Goni, F. M. (1994) *Biochem. Soc. Trans. 22*, 380S.
47. Raussens, V., Ruysschaert, J. M., and Goormaghtigh, E. (1997) *J. Biol. Chem. 272*, 262−270.
48. de Jongh, H. H., Goormaghtigh, E., and Ruysschaert, J. M. (1997) *Biochemistry 36*, 13603−13610.
49. de Jongh, H. H., Goormaghtigh, E., and Ruysschaert, J. M. (1997) *Biochemistry 36*, 13593−13602.
50. Hung, L. W., Wang, I. X., Nikaido, K., Liu, P. Q., Ames, G. F., and Kim, S. H. (1998) *Nature 396*, 703−707.
51. Rosenberg, M. F., Callaghan, R., Ford, R. C., and Higgins, C. F. (1997) *J. Biol. Chem. 272*, 10685−10694.
52. Englander, S. W., and Kallenbach, N. R. (1983) *Q. Rev. Biophys. 16*, 521−655.
53. de Jongh, H. H., Goormaghtigh, E., and Ruysschaert, J. M. (1996) *Anal. Biochem. 242*, 95−103.
54. Sturgis, J., Robert, B., and Goormaghtigh, E. (1998) *Biophys. J. 74*, 988−994.
55. Downer, N. W., Bruchman, T. J., and Hazzard, J. H. (1986) *J. Biol. Chem. 261*, 3640−3647.
56. Earnest, T. N., Herzfeld, J., and Rothschild, K. J. (1990) *Biophys. J. 58*, 1539−1546.
57. Dempsey, C. E., and Butler, G. S. (1992) *Biochemistry 31*, 11973−11977.
58. Challou, N., Goormaghtigh, E., Cabiaux, V., Conrath, K., and Ruysschaert, J. M. (1994) *Biochemistry 33*, 6902−6910.

59. Sami, M., and Dempsey, C. (1988) *FEBS Lett. 240*, 211−215.
60. Pastrana, B., Mautone, A. J., and Mendelsohn, R. (1991) *Biochemistry 30*, 10058−10064.
61. Vandenbussche, G., Clercx, A., Curstedt, T., Johansson, J., Jornvall, H., and Ruysschaert, J. M. (1992) *Eur. J. Biochem. 203*, 201−209.
62. Vandenbussche, G., Clercx, A., Clercx, M., Curstedt, T., Johansson, J., Jornvall, H., and Ruysschaert, J. M. (1992) *Biochemistry 31*, 9169−9176.
63. Alvarez, J., Lee, D. C., Baldwin, S. A., and Chapman, D. (1987) *J. Biol. Chem. 262*, 3502−3509.
64. le-Coutre, J., Narasimhan, L. R., Patel, C. K., and Kaback, H. R. (1997) *Proc. Natl. Acad. Sci. U.S.A. 94*, 10167−10171.
65. Haris, P. I., Chapman, D., and Benga, G. (1995) *Eur. J. Biochem. 233*, 659−664.
66. Bryson, E. A., Rankin, S. E., Goormaghtigh, E., Ruysschaert, J. M., Watts, A., and Pinheiro, T. J. (2000) *Eur. J. Biochem. 267*, 1390−1396.
67. Muga, A., Mantsch, H. H., and Surewicz, W. K. (1991) *Biochemistry 30*, 2629−2635.
68. Raussens, V., Narayanaswami, V., Goormaghtigh, E., Ryan, R. O., and Ruysschaert, J. M. (1996) *J. Biol. Chem. 271*, 23089−23095.
69. Loo, T. W., and Clarke, D. M. (2000) *J. Biol. Chem. 275*, 5253−5256.

BI010017+